Misan Journal of Engineering Sciences ISSN-E: 2957-4250
Vol. 4, No. 2, Dec 2025 ISSN: 2957-4242

Numerical Evaluation of Porous Media Influence on Heat Transfer Performance in Shell-and-Tube Heat Exchangers

Muntadher H. Mohammed*[1],

[1] *Department of Mechanical Engineering, Islamic Azad University of Science and Research Branch, Tehran, Iran*
**Corresponding author E-mail:* enginman3@gmail.com

(Received 10 July, Revised 12 Sep, Accepted 7 Oct)

Abstract: This study investigates the impact of porous media on the thermal and hydraulic performance of a shell-and-tube heat exchanger using computational fluid dynamics and advanced statistical optimization. The effects of varying porosity on Nusselt number, pressure drop, and heat transferred were systematically evaluated through a Central Composite Design approach, analyzed using Response Surface Methodology, and optimized via multi-objective genetic algorithms. Results demonstrate a nonlinear relationship between porosity and both heat transfer and pressure loss: while intermediate porosity levels (approximately 0.6–0.7) maximize the Nusselt number and heat exchanged, high porosity leads to diminishing returns. Pressure drop monotonically decreases with increasing porosity, with a significant trade-off observed between thermal enhancement and hydraulic cost. Contour analyses reveal that incorporating porous media leads to notably more uniform velocity and temperature fields, enhancing thermal homogenization but raising maximum system pressure by over 30%. The average shell-side temperature was reduced by 6°C in porous-enhanced cases. These findings underscore the necessity of multi-objective optimization to achieve an optimal balance between thermal performance and pressure loss in the design of next-generation heat exchangers. The study provides comprehensive insights for engineers aiming to leverage porous media for efficient thermal system design.

Keywords: Shell-and-Tube Heat Exchanger; Porous Media; CFD Simulation; Heat Transfer Enhancement; Thermal Performance.

1. Introduction

Heat exchangers are among the most widely used devices in chemical processes and thermal engineering, playing a vital role in the transfer of heat between two or more fluids at different temperatures. The operation may involve liquid-liquid, gas-gas, or gas-liquid phases, serving purposes such as cooling hot fluids, heating colder fluids, or both. Heat exchangers are extensively applied across a wide range of industries, including power plants, refineries, petrochemicals, manufacturing, process industries, food and pharmaceuticals, metal processing, HVAC, refrigeration, and aerospace. Typical applications involve systems such as boilers, steam generators, condensers, evaporators, cooling towers, preheaters, radiators, furnaces, and oil coolers. In general, a heat exchanger is defined as a device that recovers heat between two process streams.

DOI: https://doi.org/10.61263/mjes.v4i2.184

Designing various types of heat exchangers is a significant area of industrial engineering, often involving complex and time-consuming calculations. Traditionally, the design process required multiple assumptions and iterative methods following specific standards to determine optimal exchanger dimensions. However, with the advent of computer-aided tools, these calculations have become automated, significantly reducing the designer's workload to specifying operating conditions and fluid properties. Nonetheless, accurate and cost-effective design requires a thorough understanding of heat exchanger fundamentals, particularly the mechanisms of heat transfer involved.

Given the importance of porous media in diverse industries, considerable research has been conducted on heat transfer in such systems. For instance, Loryat and Ghafir [1] demonstrated that the use of porous media can enhance heat and mass transfer in energy systems, reporting Nusselt numbers approximately 50 % higher than those for laminar flows in non-porous channels.

Further work by Yang and Vafai [2] examined the influence of multiple heated blocks in a two-dimensional channel, revealing that smaller, more widely spaced blocks yielded better heat transfer performance.

Several studies have explored heat transfer enhancement using porous media due to their high fluid–solid interfacial area [3,4]. Notably, Huang and Vafai [5], through a vorticity function approach, showed that substantial heat transfer improvements are achievable with multiple porous blocks in parallel-plate channels. Powell and Mohammed [6], combining experimental and numerical methods, found that embedding porous inserts in gas heat exchangers could significantly enhance heat transfer with a reasonable pressure-drop penalty. These findings reinforce the role of porous media as highly effective heat sinks.

Yucel et al. [7] studied convective cooling enhancement of heated elements in parallel channels using porous inserts, reporting increased heat transfer with higher matrix conductivity and a rapid pressure-drop rise at elevated Reynolds numbers. Additional computational fluid dynamics (CFD) studies, such as Hobbs et al. [8], examined static mixing devices, while Kumar et al. [9] investigated Kenics static mixer performance across a wide range of Reynolds numbers and proposed new correlations for pressure drop.

Recent numerical work by Jamaarani [10] focused on turbulent-flow heat transfer in double-pipe heat exchangers filled with metallic porous media. Results indicated that lowering porosity, increasing pore diameter, and using highly conductive materials such as copper all improve heat transfer, with the overall heat transfer coefficient potentially increasing by up to seven times compared to conventional designs. However, energy loss due to increased pumping power was significant, which could be mitigated by optimizing the pore diameter.

Many researchers have investigated ways to optimize geometry and structure to further increase heat exchanger efficiency and reduce pressure losses [11–13]. For instance, studies have proposed a dimensionless analysis for curved tubes [14], new friction-factor correlations [15,16], and CFD-driven optimization for shell-and-tube arrangements with various inserts and baffles [15,17–19].

On the subject of heat transfer in metallic foams and porous materials, numerous experimental and numerical investigations have been undertaken. Free-convection heat transfer in high-porosity metal foams has been addressed by several researchers [20,21], who have systematically explored the effects of relative density, pore size, orientation, and radiative heat transfer. In general, increasing porosity tends to reduce heat transfer, while lower pore density and horizontally oriented foams provide better performance.

Further numerical studies have addressed forced convection in foam-filled channels [22], jet impingement cooling [23], and the use of nanofluids in foam-based heat sinks [24]. These works collectively demonstrate that filling channels or heat sinks with metal or composite foams significantly

enhances heat transfer, although it may be accompanied by an increased pressure drop depending on structural properties. Optimization of pore size, porosity, orientation, and matrix material is therefore crucial for performance improvement.

Recent research has also focused on innovative enhancements, such as using nanofluids [25] or optimized turbulence promoters and inserts in shell-and-tube and double-pipe exchangers [26], consistently showing meaningful thermal and hydraulic performance improvements. For example, Awais et al. [25] reported up to a 48% improvement in heat transfer using nanofluids.

These diverse investigations confirm the growing importance and potential of porous materials and advanced configuration modifications in improving heat exchanger performance across a wide range of industrial and engineering applications.

Esmaeilirad et al. [27] numerically explored heat transfer enhancement in shell-and-tube heat exchangers using porous media. A 3D CFD model with the k–ε turbulence closure simulated flow and thermal fields for porous inserts placed either in the shell or the tubes. In the shell case, the tube bundle was wrapped in porous material; in the tube case, inserts were positioned either along the central axis or attached to the inner wall. Parametric studies on porosity and dimensions showed that shell-side porous wraps could increase heat transfer significantly while limiting pressure drop. Tube-centered inserts caused excessive hydraulic loss with minimal thermal gains, whereas wall-attached inserts achieved both high heat transfer and acceptable pressure penalties.

In 2023, Rydalina et al. [28] combined experimental tests and theoretical modeling to evaluate porous aluminum inserts in shell-and-tube heat exchangers. Leveraging the high surface area of porous metals, they placed inserts in the inter-tube space and measured the resulting thermal performance. Experimental data were used to derive a similarity equation for the Nusselt number, enabling direct calculation of the heat transfer coefficient and overall heat transfer rate for flows through porous media. The methodology employed a cluster model to estimate the effective heat exchange area on the coolant side, allowing integration of geometric and material parameters into predictive calculations. Comparison of model predictions with measured data confirmed strong agreement, validating the criterion equation's applicability. Their findings support the practicality of porous metals in industrial heat exchangers, providing a calculation framework that links experimental scaling laws with design-level thermal analysis.

In a similar study within the present investigation, Zolfagharnasab et al. [29] conducted a numerical evaluation of porous-filled shell-and-tube heat exchangers (STHXs) for waste heat recovery applications. Using simulation models across a range of thermofluidic conditions, they compared fully filled and partially filled porous configurations against a conventional STHX, with emphasis on identifying flow and heat transfer mechanisms that yield uniform thermal distribution rather than solely optimizing fill geometry. Both porous designs effectively eliminated interfacial thermal jumps present in the baseline configuration, producing homogeneous temperature fields and heat transfer efficiency improvements of up to 60%. This performance gain came at the cost of higher pressure drops, with the full-foam configuration presenting the highest penalty. Partially filled designs, however, reduced the pressure drop to nearly half that of the full-foam case while maintaining notable thermal benefits, making them favorable for small-scale systems where excessive hydraulic resistance is unacceptable.

Also, Osipov and Zakharenko in 2018 [30] examined the design and application of compact, energy-efficient heat exchangers fabricated from highly porous, heat-conducting metals such as copper and aluminum. These materials, characterized by open porosity exceeding 50% of a smooth-surface reference, enable thin (centimeter-scale) exchangers with high thermal performance, provided condensate is swiftly removed to prevent excess filtration resistance. The study's thermal analysis employed Fourier (Fu) and Predvoditelev (Pd) criteria to guide design evaluation. The authors discussed production methods featuring

porous, permeable inserts in recuperative devices, notably using multiple parallel heat exchange plates separated by narrow gaps. They found that performance gains could be achieved by introducing small discontinuities in the porous layers, exploiting the elevated heat transfer rates in initial fluid contact zones. In cold Belarusian climates, these air-to-air exchangers also offer high resistance to freezing, combining durability with significant energy-saving potential.

In 2024, Umyrzhan et al. [31] investigated the performance impact of porous metals in heat exchangers through combined experimental testing and theoretical modeling. Leveraging the materials' high thermal conductivity and expanded surface area, the study examined how variations in the porosity coefficient influence heat transfer efficiency. Measurements of Freon mass flow rate and transferred heat quantity revealed a linear increase in both parameters with rising porosity, indicating enhanced heat exchange capability. Mathematical analysis confirmed this trend, suggesting that optimizing porosity can directly improve both thermal and hydraulic performance. The findings reinforce the potential of porous metals to boost efficiency and energy savings, supporting their broader adoption in power, mechanical, and other industrial applications.

Despite substantial research on heat transfer enhancement in heat exchangers through the use of porous media and metallic foams, most studies have primarily focused on either simple channel geometries or laminar flow regimes. Limited attention has been given to the application of porous materials within the hot tubes of shell-and-tube heat exchangers, particularly under turbulent flow conditions that are more representative of practical industrial applications. Moreover, comprehensive parametric investigations combining different porous matrix properties, flow conditions, and their simultaneous effects on both thermal and hydraulic performance are still lacking in the existing literature. Accordingly, the present study aims to address these gaps by numerically analyzing the impact of inserting porous media into the hot tubes of a shell-and-tube heat exchanger using CFD simulations. The objectives of this research are to evaluate the effect of porous layer properties on heat transfer augmentation and pressure drop, to identify optimal configurations that enhance overall exchanger performance, and to provide practical design recommendations based on the obtained results using design of experiments and response surface methodology.

2. Methodology

In this study, the methodology is centered on a shell-and-tube heat exchanger in which the conventional hot-water tubes are replaced with tubes filled with porous media. The thermal and hydraulic performance of this modified heat exchanger is investigated using computational fluid dynamics (CFD) simulations. The numerical approach enables a detailed analysis of the effects of porous media on heat transfer rates and pressure drop under various operating conditions. All simulations are designed to accurately represent practical scenarios and provide comprehensive insights into the underlying physical phenomena.

2.1 Shell & Tube heat exchanger

A shell-and-tube heat exchanger consists of an array of tubes enclosed within a larger cylindrical shell. Typically, one fluid flows through the tubes, while a hotter fluid passes around the tubes within the shell. The fluid types and flow arrangements can vary based on application requirements. Due to their high efficiency in accommodating multiple tubes, these heat exchangers facilitate considerable heat exchange between fluids. They are considered the most widely used type of heat exchanger in industry, primarily

owing to their ability to operate at elevated temperatures and pressures, combined with high durability and relatively few operational drawbacks compared to alternative designs. The tubes are most commonly manufactured from copper; however, depending on the operating environment, materials such as brass, aluminum, stainless steel, or nickel may also be used. Figure 1 illustrates the main components of a shell-and-tube heat exchanger, including tube sheets, baffles, and other essential elements [32].

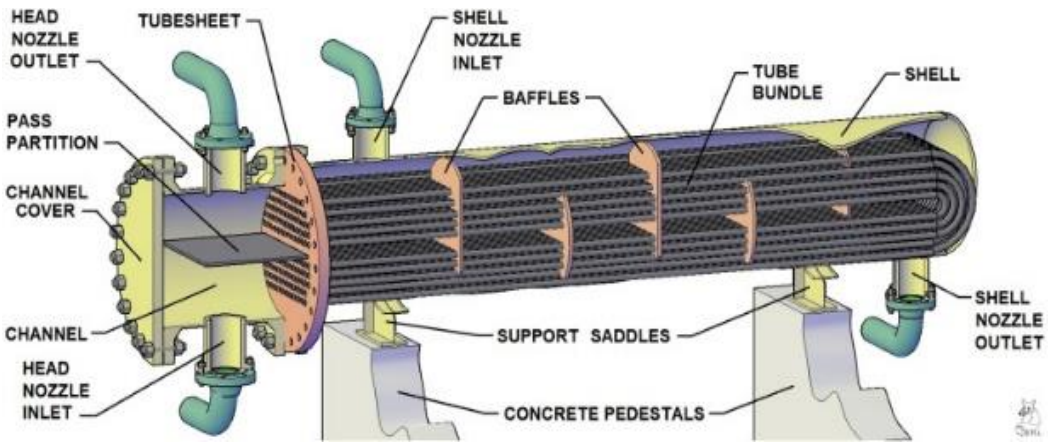

Fig. 1 Schematic of a heat and tube heat exchanger[32]

In operation, two fluids at different initial temperatures enter the exchanger—one through the tubes and the other through the shell—ensuring indirect contact. Heat transfers from one fluid to the other across the tube walls, which sometimes results in heating the shell-side fluid and other times cooling it, depending on the process configuration. Both phases, liquid or gas, can be circulated on either the tube or shell sides. When only liquids or only gases flow on both sides, the device is classified as a single-phase heat exchanger. Conversely, in applications such as boilers (for vaporization) or condensers (for condensation), which typically involve phase changes in the shell, the system is referred to as a two-phase heat exchanger.

The tube ends are fixed into tube sheets, which separate the shell space from the tube space and connect to header plenums located at either end of the exchanger. Internal baffles are usually incorporated within the shell to direct the flow, create turbulence, and enhance both heat transfer and fluid distribution over the tube bundle. This design increases contact time and improves overall exchanger effectiveness [32].

Tube arrangements may be straight or U-shaped. Straight tubes can be configured for one, two, or four passes, reflecting the number of times fluid travels across the exchanger length within the tubes. For example, a single-pass design allows fluid to flow in at one end and out at the opposite end. U-tube designs typically correspond to two-pass exchangers. Although U-tube shell-and-tube exchangers offer certain advantages, such as thermal compensation, manufacturers often prefer straight-tube designs—especially for higher capacities—due to their greater mechanical strength and lower risk of failure at tube bends. As a result, U-tube designs are generally reserved for smaller-capacity applications.

Among various operational modes, the counter-flow arrangement yields the highest thermal efficiency, as it maximizes the logarithmic mean temperature difference (LMTD) between the fluids. The counter-flow mode can increase the cold fluid's outlet temperature above the hot fluid's exit temperature, thereby improving the exchanger's effectiveness.

The design and analysis of all heat exchangers are fundamentally based on the following heat transfer

equation [32]:

$$q = U \times A \times \Delta T_{LMTD} \quad (1)$$

Where q is the total heat transferred, U is the overall heat transfer coefficient, A is the heat exchange surface area, and ΔT_{LMTD} is the logarithmic mean temperature difference. Enhancing any of these parameters directly increases the total heat transferred across the exchanger.

2.2 Geometry Overview

The current study employs a heat exchanger based on the thermos-lab setup at SRBAU, which is under active development. As illustrated in Figure 2, the simplified geometry and dimensions represent a shell-and-tube heat exchanger configuration. The design includes two separate chambers for hot and cold flow, with baffles implemented to improve cold-water circulation, and twenty-one tubes designated for the hot flow. The simplified model is used to enhance simulation robustness and reduce computational run time. The geometry outlined in Figure 2 is employed in CFD simulations utilizing the porous-media modeling approach. Further details regarding the simulation setup and methodology are discussed in the following sections.

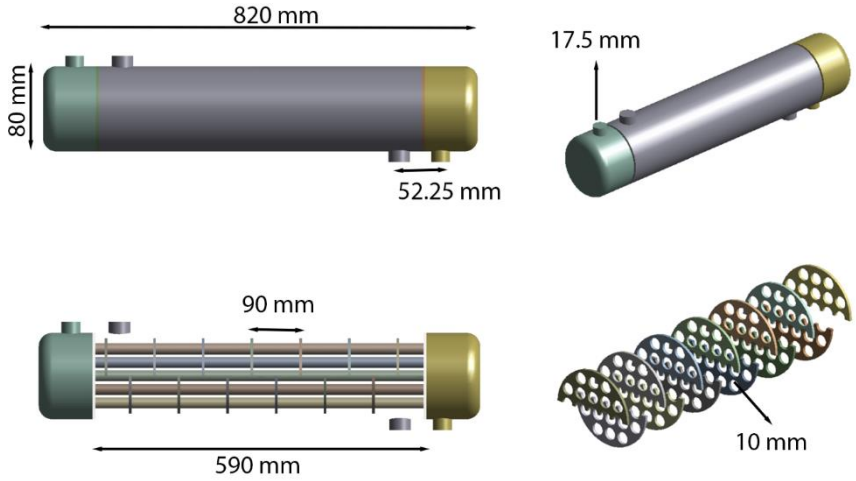

Fig. 2 Dimensions of the simplified geometry

2.3 Numerical simulation procedure

This study presents a three-dimensional numerical model for turbulent flow and heat transfer in a shell-and-tube heat exchanger with porous inserts on the tube side. The conservation of mass ensures that the rate of fluid accumulation in any control volume match es the net mass flux entering or leaving the volume: [28]

$$\partial p/\partial t + \nabla.(\rho u) = 0 \quad (2)$$

where ρ is the fluid density and u is the velocity field. This equation describes the balance of momentum, accounting for pressure, viscous forces, turbulence, and body forces in the fluid domain:[33]

$$\frac{\partial(\rho u)}{\partial t} + \nabla.(\rho uu) = -\nabla p + \nabla.(\mu_{eff} \nabla u) + F_b \quad (3)$$

Here, p is pressure; μ_{eff} is the sum of molecular and turbulent viscosities; F_b denotes body forces (e.g., gravity).For regions filled with porous media, additional drag terms are included to account for flow resistance induced by the solid matrix:[34]

$$\frac{\partial(\rho \mathrm{u})}{\partial \mathrm{t}}+\nabla.(\frac{\rho \mathrm{uu}}{\varepsilon})=-\nabla p+\nabla.(\mu_{\mathrm{eff}}\ \nabla \mathrm{u})-\frac{\mu}{\mathrm{k}}\mathrm{u}-\mathrm{C_F}\rho\left|\mathrm{u}\right|\mathrm{u} \tag{4}$$

where ε is porosity, K is permeability, and C_F is the inertial drag coefficient.
This equation governs the conservation of energy, including convection, conduction, possible source/sink terms, and, in porous domains, effective properties:[34]

$$\frac{\partial(\rho\, \mathrm{c_p\ T})}{\partial \mathrm{t}}+\nabla.(\rho\, \mathrm{c_p uT})=\nabla.(k_{\mathrm{eff}}\ \nabla \mathrm{T})+\mathrm{S_h} \tag{5}$$

where c_p is specific heat, is T temperature, k_{eff} is the effective (possibly volume-averaged) conductivity, and S_h represents volumetric sources.
For solid walls (tubes, baffles), energy transport is solely by conduction:[33]

$$\rho s\ \mathrm{c_{p,s}}\frac{\partial \mathrm{T_s}}{\partial t}=\nabla.(k_{\mathrm{s}}\ \nabla \mathrm{T_s}) \tag{6}$$

At the interface between fluid and solid domains, conservation of heat flux is enforced:[33]

$$-k_f\left(\frac{\partial \mathrm{T_f}}{\partial n}\right)_{\mathrm{int}erface}=-k_s\left(\frac{\partial \mathrm{T_s}}{\partial n}\right)_{\mathrm{int}erface} \tag{7}$$

Where the subscripts f and s represent fluid and solid, respectively; n is the direction normal to the interface.

This study employs the Generalized *k–ω* (GEKO) two-equation turbulence model, renowned for its accuracy in capturing near-wall flow features [35]. Developed by Menter in 2019 [36], the GEKO model combines the strengths of the *k–ε* closure in free-stream regions with the reliable performance of the *k–ω* approach near surfaces. By integrating transport terms into the eddy-viscosity formulation, it effectively predicts flow separation and adverse pressure gradients. The model solves two equations to compute the turbulent kinetic energy (*k*) and the specific dissipation rate (*ω*), as illustrated in Equations 24 and 25 [37].

$$\frac{\partial(\rho \mathrm{k})}{\partial \mathrm{t}}+\frac{\partial(\rho u_i \mathrm{k})}{\partial \mathrm{x}_i}=p_k-C_\mu \rho k\omega+\frac{\partial}{\partial \mathrm{x}_j}\left[\left(\mu+\frac{\mu_t}{\sigma_k}\right)\frac{\partial \mathrm{k}}{\partial \mathrm{x}_j}\right] \tag{8}$$

$$\frac{\partial(\rho\omega)}{\partial \mathrm{t}}+\frac{\partial(\rho u_i \omega)}{\partial \mathrm{x}_i}=C_{\omega 1} f_1 \frac{\omega}{k} p_k-C_{\omega 2} f_2 \rho\omega^2+\rho f_3 CD+\frac{\partial}{\partial \mathrm{x}_j}\left[\left(\mu+\frac{\mu_t}{\sigma_k}\right)\frac{\partial \omega}{\partial \mathrm{x}_j}\right] \tag{9}$$

In Equation 8, the left-hand side represents the transient and convective terms of the turbulent kinetic energy (*k*), while the right-hand side comprises the diffusion, production, and dissipation terms. Meanwhile, Equation 9 includes three terms on the right that represent the key processes, with two additional terms on the left associated with the disturbed frequency. This equation also introduces a cross-diffusion term acting as a source term to facilitate the transition from *ε* to *ω*. Default model constants were used [35]. The GEKO model's accuracy in capturing the boundary layer resolution is described in [35], which highlights the effect of the y^+ value on the results. To predict the boundary layer around the aircraft body efficiently using a

selected turbulence model, grid expansion in the domain is maintained at ($y^+ < 1$) to accurately resolve the near-wall region. Complex fluid flow equations are solved using the finite volume-based ANSYS Fluent.

To systematically investigate the effects of influential parameters and optimize the thermal-hydraulic performance of the shell-and-tube heat exchanger, a combined Design of Experiments (DOE), Response Surface Methodology (RSM), and Multi-Objective Genetic Algorithm (MOGA) approach was adopted. Statistical analysis using correlation matrices was also performed to understand parameter interdependencies. DOE provides a structured framework for conducting simulations at carefully selected points in the design space, enabling efficient exploration of model input variability. In this study, a Central Composite Design (CCD) was employed, with controllable factors including, for example, porous media porosity (ε), permeability (K), tube Reynolds number (Re_t), and solid thermal conductivity (k_s). For each case, the general form is [38]:

$$y = f(X_1, X_2, \ldots, X_n) \tag{10}$$

where y is the response and X_i These are the input variables. Also, RSM is used to construct a surrogate model that captures the relationship between input factors and output responses (e.g., Nusselt number, pressure drop, thermal performance factor). The second-order polynomial model is commonly employed:[38]

$$y=\beta_o + \sum_{i=1}^{k} \beta_i x_i + \sum_{i=1}^{k} \beta_{ii} {x_i}^2 + \sum_{i<j}^{k} \beta_{ij} x_i x_j + e \tag{11}$$

Where β_0 is the intercept, $\beta_i, \beta_{ii}, \beta_{ij}$ are regression coefficients, and e is the error term. Statistical analysis of variance (ANOVA) tests model significance and helps screen for influential parameters. A correlation matrix quantitatively expresses the pairwise linear dependencies between parameters and between input factors and responses. The Pearson correlation coefficient is given by:[38]

$$r_{xy} = \frac{\sum_{i=1}^{n} \left(X_i - \overline{X}\right)\left(Y_i - \overline{Y}\right)}{\sqrt{\sum_{i=1}^{n} \left(X_i - \overline{X}\right)^2} \sqrt{\sum_{i=1}^{n} \left(Y_i - \overline{Y}\right)^2}} \tag{12}$$

Where X and Y are the variables of interest. To ensure computational accuracy, all governing equations were discretized using the Finite Volume Method (FVM). The convection terms were approximated using the second-order upwind scheme, which minimizes numerical diffusion and improves the precision of solutions, particularly for flows with strong gradients.

For pressure–velocity coupling, the Coupled algorithm was employed, enabling the simultaneous solution of the momentum and continuity equations. This approach enhances both stability and convergence rate, especially for complex flows exhibiting strong coupling between pressure and velocity fields.

Spatial gradients and variable interpolations at cell faces were determined using the least-squares cell-based reconstruction method. This technique computes gradients by minimizing the squared differences between cell-center values and neighboring nodes, providing improved accuracy on unstructured and non-orthogonal grids.

The resulting system of algebraic equations was solved iteratively until the residuals for all variables fell below 10^{-6}, and solution variables reached steady-state convergence.

2.4 Boundary Condition

In this study, the computational domain comprises a shell-and-tube heat exchanger with distinct cold and hot fluid streams, each entering and exiting through dedicated inlets and outlets. The simulation is conducted as a two-fluid problem, enabling a detailed evaluation of heat transfer between the shell and tube sides. Both the cold and hot fluid inlets are assigned prescribed mass flow rate boundary conditions, ensuring fully controlled and constant flow rates for each stream throughout the simulation. At the outlets, the pressure is set to atmospheric conditions, allowing the flow to exit freely while maintaining numerical stability.

In this study, the shell-side porous structures were modeled using the porous-media approach available in the CFD solver, rather than explicitly resolving individual pores. This method replaces the geometric complexity of real porous inserts with volumetric momentum and energy source terms, enabling accurate prediction of their macroscopic thermal–hydraulic behavior while significantly reducing computational cost. The porous zones were assigned the thermo-physical properties of aluminum, consistent with the actual insert material, ensuring correct thermal conduction within the solid phase. Porosity (ε) was explicitly defined in the model to represent the volumetric fraction of void space, while viscous and inertial resistance coefficients were calibrated according to the expected permeability and structural characteristics. The secondary (bulk) viscosity effect associated with the porous medium was incorporated via an additional dissipation term in the momentum equation, capturing pressure losses linked to internal micro-scale flow resistance. This modeling framework allows a coupled evaluation of conduction through the solid matrix and convection within the pore space, accurately representing the performance of aluminum-based porous inserts without requiring full-scale microstructural resolution.

All solid surfaces, including the tube external walls, shell internal walls, and baffles, are modeled as non-adiabatic but with zero heat transfer (i.e., adiabatic condition is not imposed, but the walls do not participate in heat exchange with the external environment). No-slip velocity boundary conditions are enforced at all wall surfaces. The hot-side tubes are represented as three-dimensional porous media domains. Fixed physical properties, including a constant dynamic viscosity and an isotropic (three-dimensional) second viscosity, are set for the porous zone. The momentum and energy interactions within these domains are reflected in the governing equations as outlined in numerical modelling. Therefore, all assigned boundary conditions are shown in Figure 3.

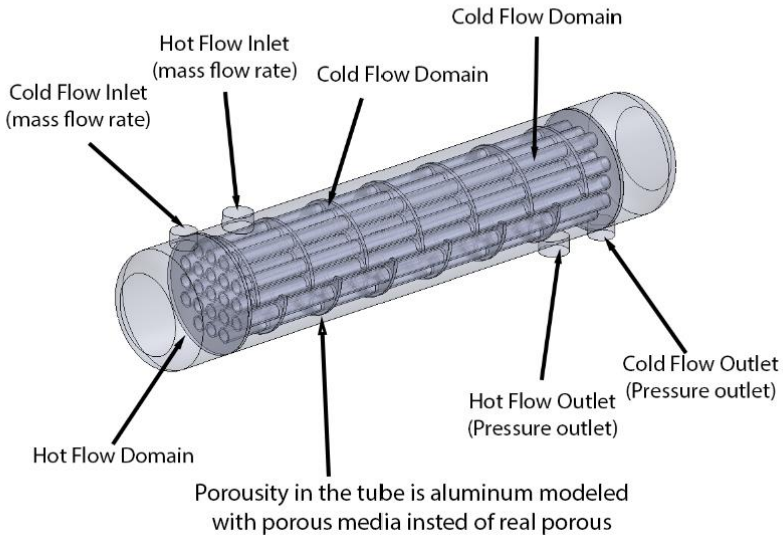

Fig. 3 Boundary Conditions of the simulation

All boundary condition specifications for the shell-and-tube heat exchanger model, including inlet mass flow rates and temperatures, outlet pressures, material properties of porous tubes, and relevant wall and interface settings, are comprehensively summarized in Table 1. This table provides a clear overview of each applied boundary, parameter values, and their locations within the computational domain.

Table 1 Boundary Condition Values

Parameter	Unit	Value
Hot flow mass flow rate	(Kg/s)	0.23
Cold flow mass flow rate	(Kg/s)	0.17
Hot flow Temperature	(K)	328.15
Cold flow Temperature	(K)	288.15
Porosity range		0.4

2.5 Grid Generation

In this study, a multi-zone computational mesh was generated for the shell-and-tube heat exchanger model, utilizing both structured and unstructured grid elements to accurately resolve critical features of the domain. Hexahedral elements were employed in the structured regions—particularly for the porous-media tubes and shell walls—while tetrahedral elements were used in the unstructured regions to capture complex geometries and interfaces. The grid design prioritized uniform element sizing in key areas, especially at the interface between the shell and tube walls where heat transfer occurs.

A grid-independence study was performed to ensure simulation accuracy and stability while maintaining computational efficiency. The effects of mesh refinement were evaluated for key performance metrics, including heat transfer rate and pressure drop. The study revealed that coarse meshes produced notable discrepancies (as shown in Figure 4), whereas fine meshes reduced variations in thermal

performance metrics to less than 5%. For instance, the total number of mesh cells in the finest discretization was approximately 3,300,000, ensuring high fidelity in capturing the thermal–hydraulic interactions between the cold and hot flow streams.

The final mesh configuration, shown in Figure 5, adequately resolves the porous-medium regions, fluid domains, and interface boundaries, confirming its suitability for accurate CFD simulation. These findings underscore the critical influence of mesh resolution on capturing essential flow and heat transfer phenomena in heat exchanger studies and validate the selected mesh density for subsequent parametric and optimization analyses.

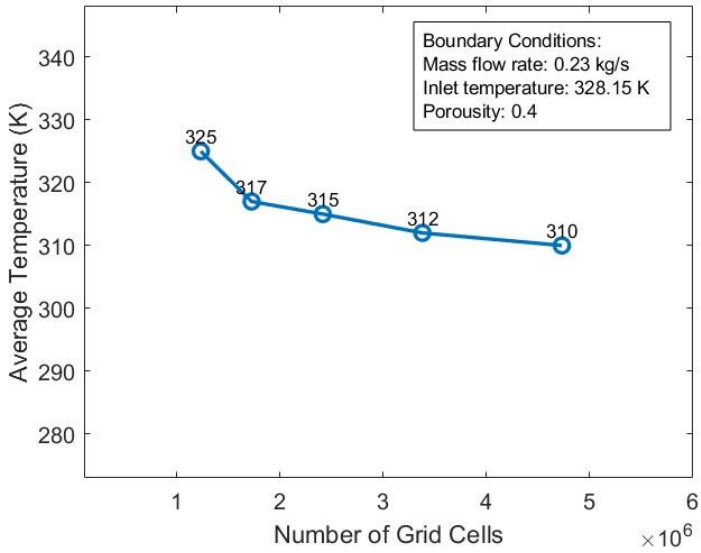

Fig. 4 Grid independence study

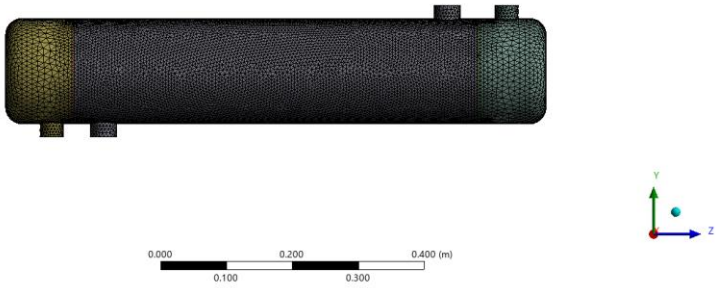

Fig. 5 Mesh grid over simulation domain

3. Results& Discussion

This section presents and analyzes the numerical results obtained for the shell-and-tube heat exchanger configuration featuring porous media on the tube side. The CFD simulations employ advanced multi-zone

meshes and robust numerical methods to ensure accurate prediction of both thermal and hydraulic behavior across a range of operating conditions. To verify the credibility of the developed model, a detailed grid-independence study was performed, confirming the reliability of the chosen mesh resolution for capturing key flow and heat transfer phenomena.

Model validation was achieved by comparing the simulation results with experimental data from the double-tube heat exchanger study conducted by Marzouk et al. [26]. The close agreement between the CFD predictions and experimental benchmarks confirms the accuracy of the present numerical approach. Following validation, a comprehensive investigation of the effects of porous-media parameters, flow conditions, and geometric features on heat exchanger performance was conducted. The findings provide valuable insights into the optimal design and operation of porous tube–enhanced shell-and-tube heat exchangers.

3.1 Validation

For the three-dimensional validation case, CFD simulations were performed to evaluate the Nusselt number across a range of Reynolds numbers (3400, 3850, 4250, 4550, 5000, and 5600) within the double-tube heat exchanger configuration. The simulation setup and grid were kept consistent with those employed throughout the main study to ensure accurate and comparable results. Validation was conducted by comparing the numerically predicted Nusselt numbers with the experimental data reported by Marzouk et al. [26]. As shown in Figure 6, the comparison demonstrates strong agreement between the present simulations and the experimental measurements across the full range of investigated Reynolds numbers. This consistency confirms the robustness and accuracy of the current numerical model in predicting the thermal performance of the heat exchanger under turbulent flow conditions.

3.2 Results

In this study, the design exploitation has been performed on the shell and tube heat exchanger to evaluate the influence of porous media on thermodynamic performance by designing an experiment using the parameters introduced. In addition, the parameters are five independent of each other.

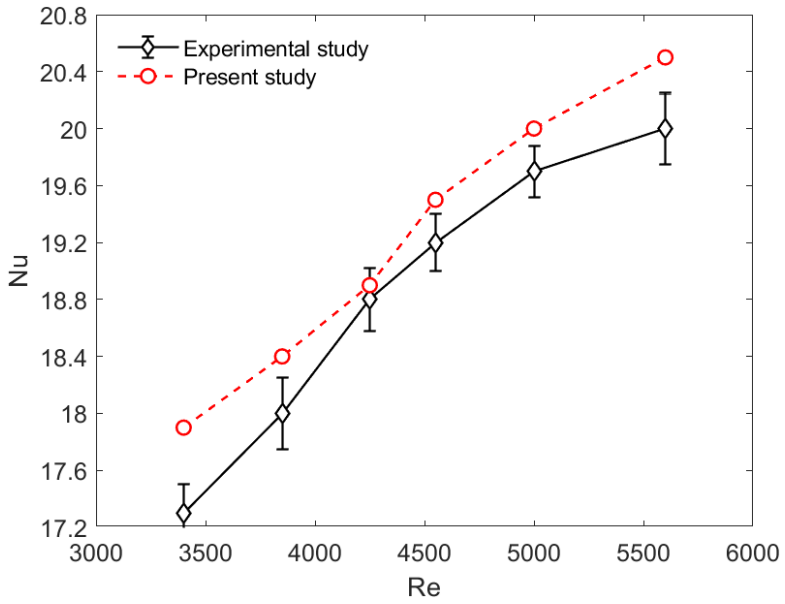

Fig. 6 Validation results for a double tube heat exchanger based on Marzouk et al.[26]

To initiate the optimization process, it is crucial to implement a suitable experimental design approach that generates a dataset that thoroughly examines the cause-and-effect relationships between input and output parameters. The statistical CCD algorithm was chosen as the experimental design methodology for this study. This algorithm is well-regarded for efficiently identifying optimal design parameters and exploring the parameter space. A comprehensive dataset was generated using CCD, enabling an in-depth analysis of the relationships between the input and output parameters. CCD is a well-established experimental design algorithm that offers numerous advantages. By employing a combination of factorial, axial, and center points, CCD enables the exploration of the entire design space while ensuring robustness and efficiency. The algorithm provides a balanced distribution of experiments, allowing for the identification of critical factors and their interactions. The CCD algorithm implemented in this study generated five experiments. These experiments were designed based on the five input parameters with predetermined ranges specified in Table 2. The experimental design aimed to comprehensively understand the cause-and-effect relationships between the input and output parameters.

Table 2 Experiment Parameters

Parameter	Type	Unit	Value
Porosity	Input	-	0-0.9
Nusselt Number	Output	-	-
Pressure Drop	Output	Pa	-
Heat exchanged	Output	W	-

Following the sampling step conducted through the design of experiments (DOE), it is essential to employ Response Surface Methodology (RSM) to establish an appropriate interpolation between design points. In this study, the Genetic Aggregation method is employed within ANSYS Workbench to develop RSM due to its ability to generate multiple solutions using a population-based approach, incorporating fitness function, selection, crossover, and mutation. RSM plays a crucial role in achieving an effective

interpolation between design points. The interactions between factors are thoroughly explored using RSM, enabling a comprehensive analysis of their combined effects. This statistical technique aids in identifying the optimal combination of input variables that yields the desired output. The Genetic Aggregation method is employed in this study to develop RSM within ANSYS Workbench. This method is selected because it can generate multiple solutions using a population-based approach. Following the simulation, a comprehensive analysis of the obtained results is conducted. In the experiment phase design, five design points were meticulously formulated using the Central Composite Design (CCD) method and subjected to computational fluid dynamics (CFD) simulations. Figure 7 visually presents the output parameter values corresponding to each meticulously designed design point. The blue line represents the Nu coefficient, while the red line corresponds to the heat exchange observed in simulations.

Figure 7 presents the variation of both the Nusselt number and the amount of heat exchanged across the five design points generated by the Central Composite Design (CCD) methodology. The horizontal axis indicates the point name (corresponding to the specific CCD design point), and the upper axis annotates the associated porosity values at each point, ranging from 0.1 to 0.9.

The left vertical axis shows the Nusselt number, while the right vertical axis corresponds to the total heat exchanged. Both quantities demonstrate significant sensitivity to changes in porosity:

Overall, the Nu value varies non-monotonically with porosity. While a gradual increase in Nu is observed from design point 2 to points 4 and 5 (porosity rising from 0.2 to 0.7), design point 1 (porosity 0.1) surprisingly exhibits a local maximum, and point 2 sees a pronounced local minimum. This behavior indicates a highly nonlinear dependence of convective heat transfer on the structure of the porous medium, likely reflecting the competing effects of increased surface area versus enhanced flow resistance at low porosities.

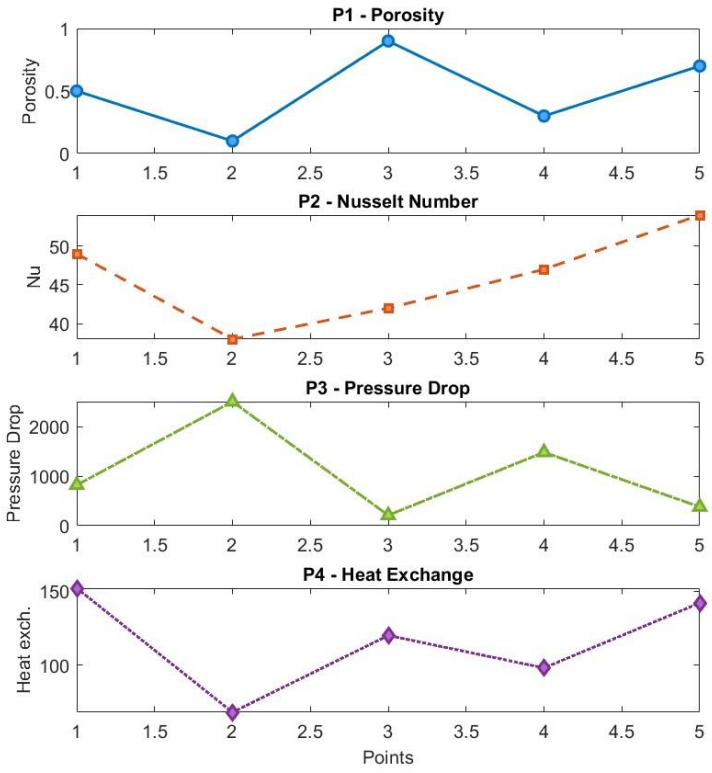

Fig. 7 Design points vs. Parameters Validation results for a double tube heat exchanger based on Marzouk et al.[26]

A similar non-monotonic trend is observed for heat exchange, peaking at design points corresponding to intermediate porosity levels (notably at points 3 and 4). A general observation is that extremely low or high porosity values are not optimal for maximizing either *Nu* or the total heat exchanged under the studied conditions.

These results underscore the critical role of porosity as a design variable and highlight the complex interplay between thermal enhancement and fluid-dynamic penalties in porous-media applications. The observed trends further emphasize the necessity of employing multifactorial design and optimization strategies—such as Central Composite Design (CCD) in conjunction with Response Surface Methodology (RSM)—to effectively explore and exploit the multidimensional design space for enhanced heat exchanger performance.

Figure 8 presents the validation of the constructed response surfaces by comparing the normalized predicted values (from the RSM models) with the corresponding observed values from CFD simulations at the five DOE design points. The analysis encompasses three key output parameters: Nusselt number (*Nu*, red squares), pressure drop (green squares), and total heat exchanged (blue squares).

All data points in Figure 8 align closely with the 1:1 correlation line, confirming strong agreement between the RSM predictions and the actual simulation results. This high degree of correlation across all three performance metrics demonstrates that the response surface models accurately capture the trends and nonlinearities inherent in the system's behavior across the explored parameter space.

Such predictive accuracy is vital for establishing confidence in subsequent optimization studies and ensuring the reliability of design recommendations derived from the RSM framework. The results indicate that the CCD sampling strategy, when combined with genetic aggregation and RSM, yields a robust and generalizable surrogate model for evaluating and optimizing heat exchanger performance as a function of porosity and other relevant design variables. Minor deviations between predicted and observed values are negligible, validating both the fidelity of the numerical simulations and the adequacy of the adopted statistical modeling approach.

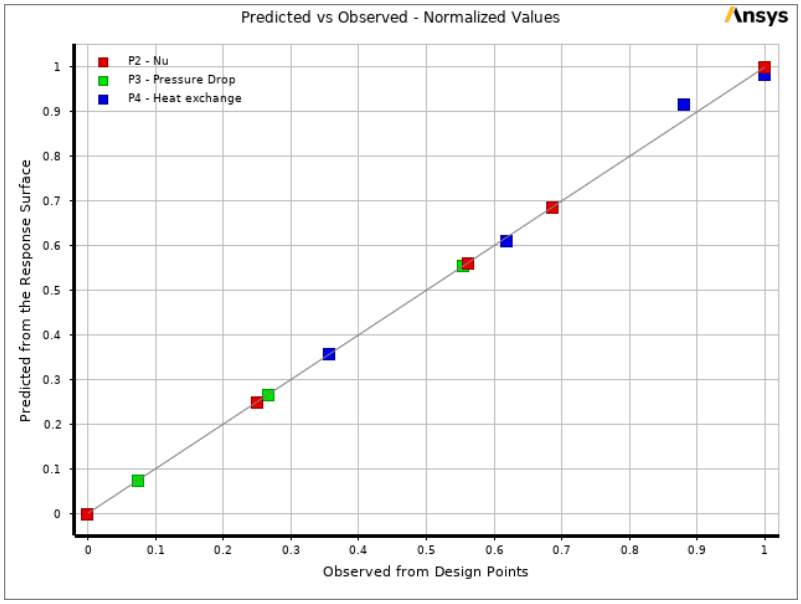

Fig. 8 Predicted vs Observed – Normalized values

Figure 9 depicts the relationship between the Nusselt number (Nu) and the porosity (P1) of t he inserted porous media within the shell-and-tube heat exchanger. This response curve provides comprehensive insight into the influence of porosity on convective heat transfer enhancement.

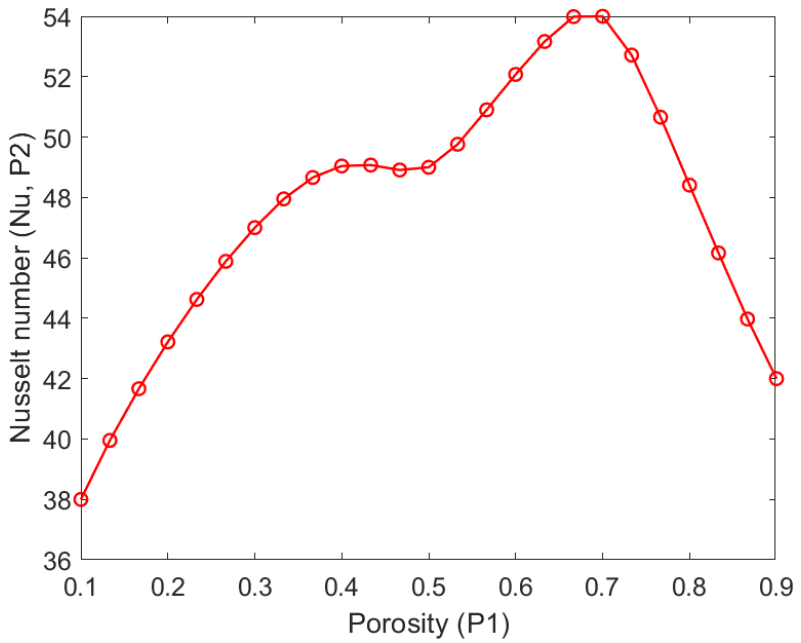

Fig. 9 Response Chart of Nusselt vs Porosity

The results exhibit a strongly nonlinear trend. As porosity increases from 0.1 to approximately 0.7, the Nusselt number rises steadily, indicating improved heat transfer performance with increasing pore volume. This enhancement can be attributed to an optimal balance between increased surface area for fluid-solid interaction and the permeability provided by moderate porosity levels, which together promote higher

convective heat transfer coefficients.

A distinct maximum is observed in the vicinity of porosity ≈ 0.7, where the Nusselt number attains its peak value. Beyond this optimum, further increases in porosity cause a rapid decline in Nu. This is likely due to the diminishing solid matrix, which reduces the available surface area for heat transfer despite lowered flow resistance. At very high porosities (above 0.8), the structure becomes too open, and the beneficial effects of turbulence enhancement and increased surface area are outweighed by the reduction in matrix presence.

These findings highlight the existence of an optimal porosity range that maximizes thermal performance for a shell-and-tube heat exchanger with porous inserts. The results also underscore the importance of careful material and structural selection during the design phase to ensure that both heat transfer and hydraulic penalties are properly balanced.

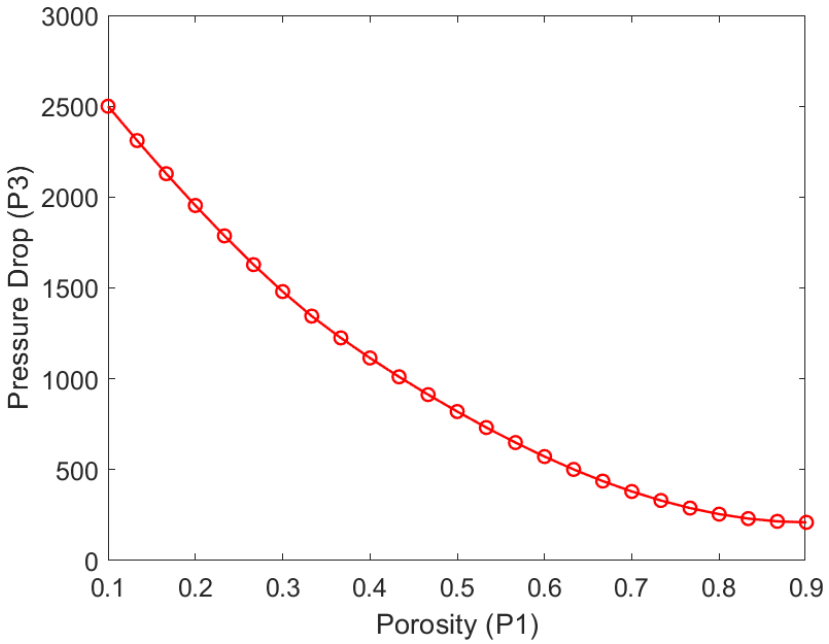

Fig. 10 Response Chart of Pressure Drop Vs Porosity

Figure 10 displays the dependence of the pressure drop (P3) on the porosity (P1) for the shell-and-tube heat exchanger with porous media inserts. The pressure drop is a key assessment parameter because it directly relates to the energy cost and pump requirements in practical heat exchanger operation.

The results illustrate a strong, monotonic decrease in pressure drop with increasing porosity across the studied range ($0.1 \leq P1 \leq 0.9$). At the lowest porosity ($P1 = 0.1$), the pressure drop reaches its maximum (approximately 2500 Pa), reflecting the substantial flow resistance imposed by the dense porous matrix. As porosity increases, the internal structure becomes more open, which substantially reduces hydraulic resistance. Consequently, the pressure drop drops sharply, approaching minimal values at the highest porosities.

This inverse relationship highlights the well-known trade-off in porous media design for heat exchangers. Lower porosity enhances surface contact and can intensify heat transfer (as discussed

previously), but it significantly increases flow resistance, resulting in higher pressure drops. Higher porosity substantially alleviates the pressure penalty, making the exchanger more energy-efficient from a pumping perspective, but often at the expense of reduced heat transfer augmentation.

Therefore, determining the optimal porosity is critical for achieving a balance between desirable heat transfer rates and acceptable operating costs. The data indicate that while intermediate porosities may offer the best compromise for thermal performance, excessively high or low porosities can be suboptimal due to penalties in either pressure drop or heat transfer.

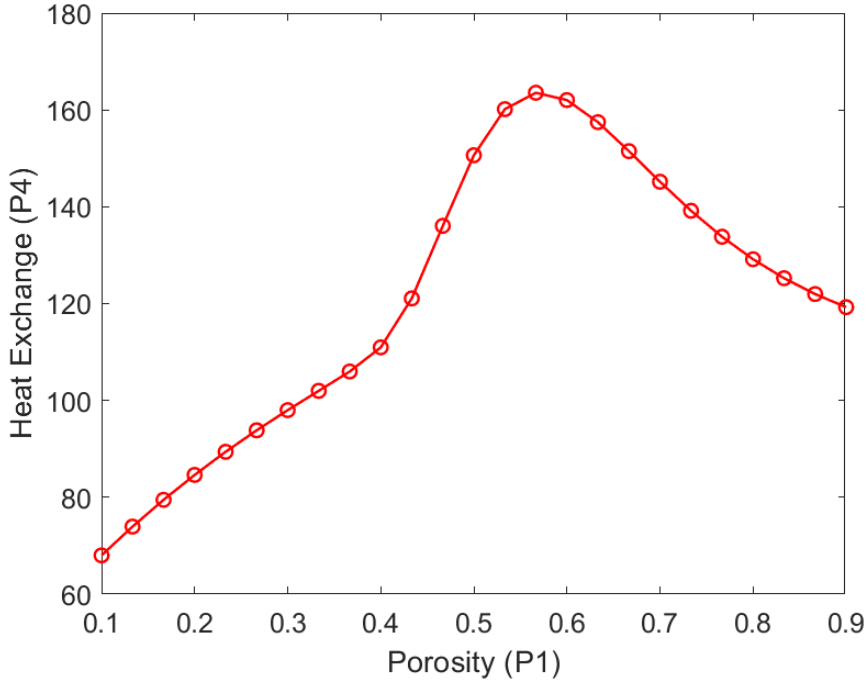

Fig. 11 Response Chart of Heat exchanged vs Porosity.

Figure 11 illustrates the variation of the total heat exchanged (P4) as a function of porosity (P1) in the shell-and-tube heat exchanger with porous-media inserts, offering a holistic view of the system's thermal performance under varying porous configurations.

The data reveal a pronounced nonlinear dependence of heat exchange on porosity. At low porosity levels (P1 = 0.1–0.4), there is a steady and continuous rise in heat exchanged, attributed to the enhanced surface area and more effective mixing of the working fluid within the densely packed porous structure. As porosity increases further (up to P1 ≈ 0.6), the rate of heat exchange growth becomes even steeper, reaching a distinct maximum at intermediate porosity levels (P1 ≈ 0.6–0.65). This range represents the optimal operational window, where the competing effects of high heat-transfer surface area and fluid accessibility are most effectively balanced.

Beyond this optimum, a marked decline in heat exchange is observed with further increases in porosity. At high porosity values (P1 > 0.7), the diminished solid matrix reduces the effective surface area for heat transfer, and the benefits of additional pore volume are outweighed by the loss of conduction pathways. Consequently, total heat exchange decreases despite lower flow resistance.

This well-defined peak emphasizes the necessity of optimizing porous-insert design: both excessively low and excessively high porosities yield suboptimal thermal performance. The results confirm that effective porous-media heat exchanger design requires targeting a specific porosity range to achieve an optimal trade-off between heat-transfer enhancement and hydraulic penalties, as corroborated by the

preceding Nusselt number and pressure-drop analyses.

Figure 12 presents the linear correlation matrix for the primary parameters investigated—porosity, Nusselt number, pressure drop, and total heat exchanged. This matrix quantitatively illustrates the magnitude and direction of linear relationships among these variables, clarifying the dependencies identified in the parametric study.

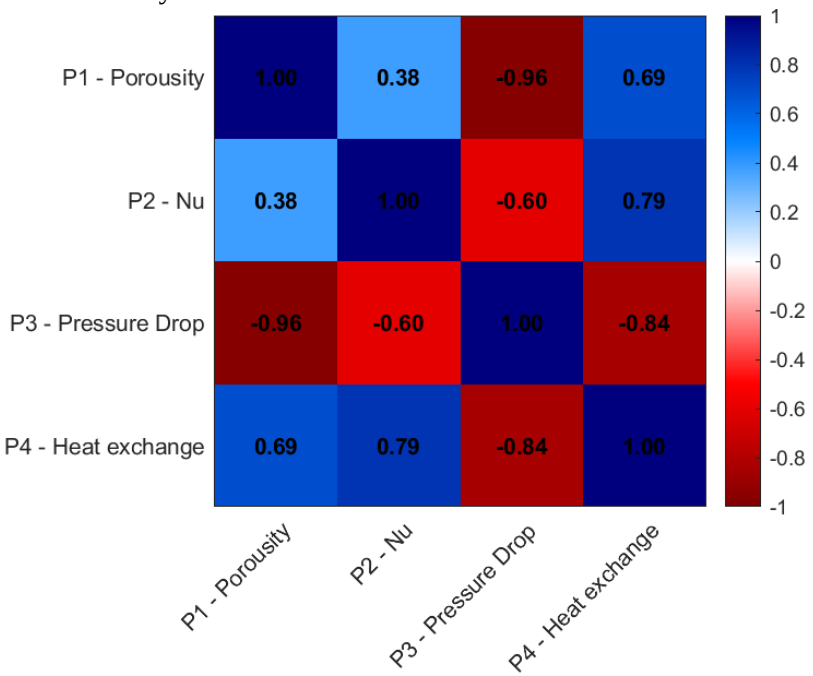

Fig. 12 Correlation matrix

As evident from the matrix, porosity exhibits a strong negative correlation with pressure drop, confirming that as porosity increases, pressure drop decreases significantly. Porosity shows a moderate positive correlation with both Nusselt number and heat exchanged, manifested by the orange-red coloration. This reflects the enhancement in heat transfer performance with increasing porosity up to an optimal range, as earlier detailed in Figures 10 and 11. Nusselt number and heat exchanged are also strongly and positively correlated, consistent with the expected physical relationship between convective heat transfer coefficient and total heat exchanged. Pressure drop is negatively correlated with both Nusselt number and heat exchanged, indicating that conditions favoring higher heat transfer efficiency tend to incur lower hydraulic penalties only up to a certain porosity, beyond which both parameters may decline.

This matrix substantiates the findings from the detailed parametric response charts. The non-linear and occasionally non-monotonic trends discussed previously are reflected in the less-than-perfect linear correlations, particularly between porosity and heat transfer measures, signaling the necessity for multi-objective optimization strategies in porous media heat exchanger design.

Figure 13 presents the quadratic determination matrix for the analyzed parameters: porosity, Nusselt number, pressure drop, and heat exchanged. This matrix goes beyond simple linear relationships by quantifying the proportion of variance in each response variable that can be explained by a second-order (quadratic) model concerning each input. Thus, it more accurately captures the inherently non-linear interactions in the system, which are especially relevant in engineering applications such as porous media heat exchangers.

From this matrix, several observations emerge: The diagonal elements, particularly for Nusselt number, are near unity (bright yellow), indicating that the majority of the variation in each primary response is well

explained by their quadratic models. Off-diagonal elements reveal notable quadratic dependencies between variables. For example, the relationship between Nusselt number and pressure drop, as well as between Nusselt number and heat exchanged, exhibits considerable quadratic determination. This supports the findings from response charts that the effect of porosity on both thermal and hydraulic performance is not merely linear, but fundamentally quadratic or higher order. The heat exchanged shows strong quadratic determination not only concerning itself, but also with Nusselt number and pressure drop, confirming that the total heat transferred is governed by a complex interplay of both heat transfer and flow resistance characteristics.

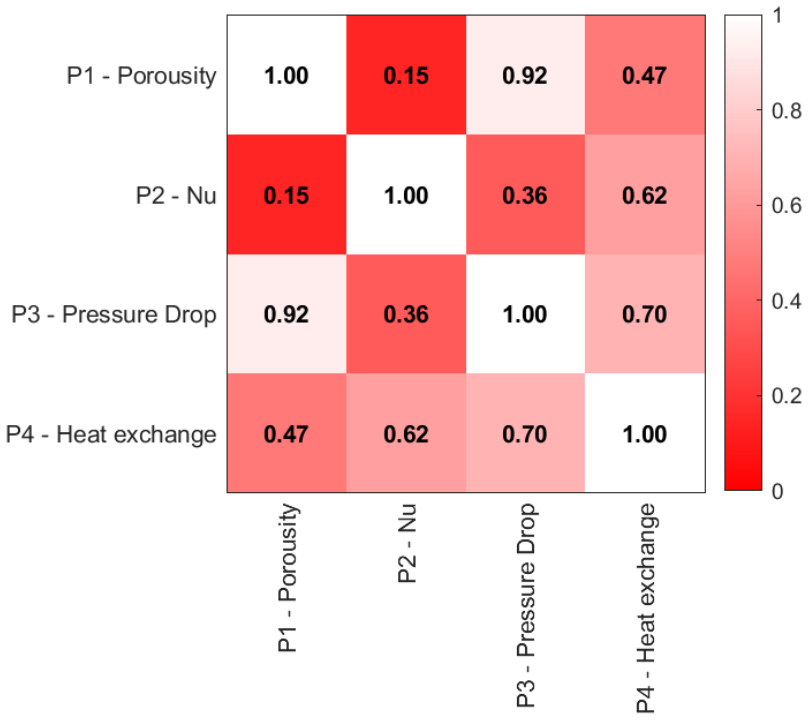

Fig. 13 Determination matrix

Table 3 summarizes the experimental results for various porosity levels, illustrating their impact on pressure drop, Nusselt number, and heat exchanged. Notably, the data reveal that a porosity of 0.4 delivers the best overall thermal performance with improved thermodynamics while maintaining a moderate pressure drop. This outcome suggests that intermediate porosity provides an effective balance between enhanced heat transfer and acceptable hydraulic resistance, confirming that neither extremely low nor very high porosity is optimal. The results underscore the importance of selecting an appropriate porosity value to optimize the thermal and hydraulic performance of shell and tube heat exchangers with embedded porous media.

Table 3 Comparison between heat exchange with and without Porous media

Case	Porosity	Nusselt	Pressure Drop	Heat Exchanged
Simple	0	38	48	96
40% porosity	0.6	50	580	160

The marked increase in pressure drop reported in Table 3 aligns with the hydraulic penalties typically observed when porous media are incorporated into heat exchanger shells. In industrial practice, several alternative configurations are employed to mitigate these penalties while maintaining high heat transfer performance. Examples include the use of segmental or helical baffles to promote cross-flow with reduced flow obstruction, tube-bundle optimization to minimize shell-side recirculation zones, and the integration of rod-baffle or grid-support designs that provide structural rigidity with minimal frontal area to the flow. Additionally, certain applications utilize multi-pass shell configurations or shell-diameter expansion sections to locally reduce velocity and pressure losses.

Although these configurations differ from the porous-media approach adopted in the present study, they represent well-established industrial strategies for achieving a balance between heat transfer enhancement and acceptable pumping requirements.

Further, the results for the 40% porosity tubes are presented. The CFD simulation results represent the Fluid Flow, Pressure, and Temperature for the 3D simulation. First, in Figure 14, the fluid flow in the domain is presented.

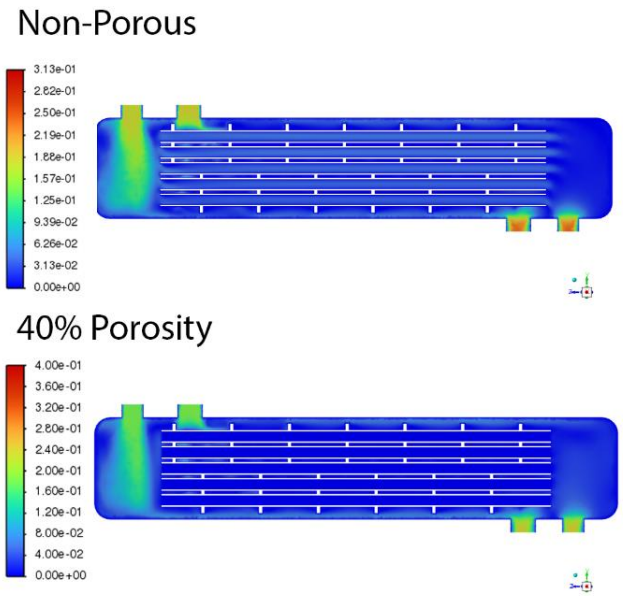

Fig. 14 Flow velocity Contours in yz plane

The comparative velocity contour plots for the shell-and-tube heat exchanger, shown in Figure 14, provide valuable insight into the influence of porous media on the local flow structure. In the absence of porous inserts, the velocity distribution within the shell side exhibits pronounced spatial non-uniformity, with elevated velocities concentrated in the core regions and lower velocities near the baffle and tube surfaces. Such non-uniformity often results in inefficient utilization of the available heat-transfer area and the formation of localized thermal gradients.

The introduction of porous media, however, markedly transforms the internal flow profile. The contours reveal that the velocity field becomes substantially more uniform throughout the shell region owing to the flow-dispersing characteristics of the porous matrix. This homogenization effect can be attributed to

enhanced flow dispersion and the suppression of large-scale recirculation zones—consistent with the findings of Nouri-Borujerdi et al. and Qi et al. [3, 4], who demonstrated the capability of porous inserts to mitigate flow maldistribution and promote more effective convective mixing.

Furthermore, the presence of the porous medium reduces the local flow-velocity magnitude within the shell-side region. This reduction primarily arises from the increased hydraulic resistance of the intricate pore structure, which dissipates kinetic energy and dampens the velocity peaks typically observed in non-porous configurations. At the same time, a modest overall increase in velocity can be observed within the tube-side domain. This phenomenon is attributed to the higher pressure differentials required to drive the fluid through the high-resistance porous zone, thereby elevating the mean velocity within the adjacent tube passages—an effect also reported by Vafai et al. [5].

In summary, the incorporation of porous media into shell-and-tube heat exchangers produces a more uniform and controlled velocity field within the shell, reduces velocity peaks due to elevated flow resistance, and—under constant mass-flow or inlet conditions—induces a slight rise in tube-side velocity as a result of pressure redistribution, as illustrated in Figure 15.

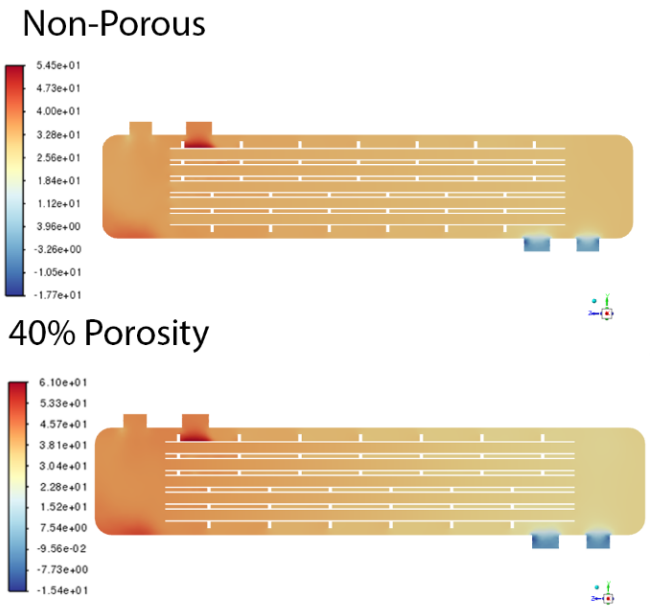

Fig. 15 Pressure Field Contours in yz plane

The pressure contour analysis provides further evidence of the significant impact of porous media integration in the shell-and-tube heat exchanger. Comparative inspection shows that while local pressure losses remain moderate throughout the shell region, the presence of a porous matrix leads to a marked increase in the overall maximum pressure within the system. Quantitatively, the simulation results indicate that the maximum pressure in the porous-media configuration is elevated by more than 30% compared to the non-porous baseline case.

This increase in peak pressure is a direct consequence of the augmented flow resistance imposed by the porous structure. As the working fluid encounters the complex network of pores, momentum losses accumulate more rapidly than in open flow, necessitating higher driving pressures to maintain a constant mass flow rate. Similar findings are reported in the literature, where the addition of porous inserts consistently correlates with both increased pressure gradients and enhanced mixing phenomena. This dual

effect is fundamental to the trade-off inherent in porous media heat exchanger design: while the porous matrix promotes superior flow distribution and heat transfer (as seen in the velocity field analysis), it simultaneously results in a greater overall pressure drop.

Therefore, when assessing the feasibility and performance of porous-media-enhanced heat exchangers, it is essential to account for this increase in system pressure. The findings underscore the importance of multi-objective optimization, where both thermal performance and hydraulic cost must be balanced to realize practical engineering solutions. These results also support the use of advanced design methodologies, such as those based on response surface methodology (RSM) and genetic algorithms, to identify optimal operating conditions that leverage the benefits of porous media without incurring prohibitive pressure penalties.

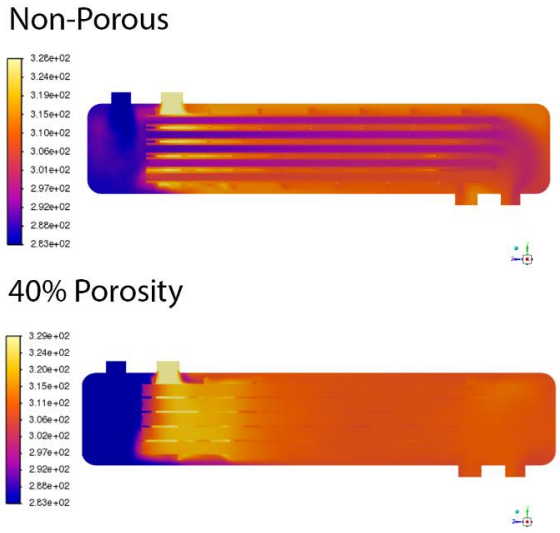

Fig. 16 Temperature Distribution Contours yz plane

The temperature contour plots present clear evidence of the beneficial effect of porous media on shell-side temperature distribution within the shell-and-tube heat exchanger. In the non-porous configuration, temperature fields typically exhibit pronounced gradients and localized hot or cold regions, which reflect poor mixing and non-uniform heat transfer. However, the introduction of porous media significantly enhances thermal homogenization, resulting in a much more uniform temperature distribution across the entire shell region. This effect stems from the increased turbulence and flow dispersion induced by the microstructure of the porous matrix, which disrupts temperature boundary layers and promotes more effective energy exchange between the working fluid and heat transfer surfaces.

Moreover, the quantitative comparison reveals that the average shell-side temperature in the porous media-enhanced case is reduced by approximately 6°C relative to the non-porous baseline. This decrease in mean temperature is a direct indicator of the improved heat extraction capability facilitated by the porous insert.

4. Conclusions

In this study, a comprehensive numerical and statistical investigation was performed to elucidate the effects of porous media on the performance of a shell-and-tube heat exchanger. By integrating Computational Fluid Dynamics (CFD) simulations with Response Surface Methodology (RSM), Central Composite Design (CCD), and optimization through a Multi-Objective Genetic Algorithm (MOGA), the study offers

a holistic understanding of both the thermal and hydraulic impacts of introducing porous structures within the shell domain. The key findings are summarized as follows:

• A comprehensive numerical and statistical framework combining CFD, RSM, CCD, and MOGA was developed to evaluate the influence of porous media on shell-and-tube heat exchanger performance.

• Porosity exhibited a strongly nonlinear influence on performance metrics, with optimal thermal performance achieved within a porosity range of approximately 0.6–0.7.

• **Thermal–hydraulic trade-off:** The Nusselt number and heat transfer rate increased with porosity up to the optimum range, while pressure drop decreased steadily—but with diminishing thermal gains beyond the optimal point.

• Porous media induced more uniform velocity and temperature distributions, minimized hot and cold spots, and enhanced fluid mixing, resulting in an average 6 °C reduction in shell-side temperature.

• The integration of porous structures caused moderate local pressure losses but led to an overall increase of more than 30% in maximum system pressure due to additional flow resistance.

• Multi-objective optimization using RSM and MOGA successfully identified design regimes that balanced thermal enhancement with hydraulic efficiency.

• Quadratic response models were validated, confirming significant nonlinearities and interdependencies among key parameters.

• The results emphasize the necessity of careful selection of porosity and structural characteristics to maximize heat transfer while minimizing hydraulic penalties.

• Future work should include experimental validation, exploration of alternative porous materials and geometries, and extension of the methodology to transient and multiphase flow applications.

Nomenclature:

A Heat transfer area (m^2)

C_f Inertial drag coefficient (1/m)

C_p Specific heat at constant pressure J/(kg·K)

DOE Design of Experiments

Fb Body force vector (m/s^2)

K Permeability m^2

K_eff Effective thermal conductivity (W/(m·K)

k Thermal conductivity (general) (W/m·K)

k_s Solid thermal conductivity W/(m·K)

n Unit vector normal to surface (dimensionless)

q Heat transfer rate (W)

Re Tube Reynolds number (dimensionless)

RSM Response Surface Methodology

S_h Volumetric heat source term (W/m^3).

T Temperature (°C)

U Overall heat transfer coefficient ($W/(m^2·K)$

y^(+1) Non-dimensional wall distance (dimensionless)

ΔT Log mean temperature difference (°C)

ΔP Pressure Drop (Pa)

Greek Symbols

β_0 Regression coefficients in RSM model (dimensionless)

ε Porosity (dimensionless)

μ Dynamic viscosity Pa·s (kg/(m·s)

μ_b Second (bulk) viscosity (Pa·s)

μ_eff Effective viscosity (molecular + turbulent) Pa·s (kg/(m·s)

ρ Fluid density kg/m^3

Subscripts

b Baffle

c Cold

eff Effective

f Fluid (pure water)

h Hot

nf Nanofluid

p Nanoparticle

s Solid

Acknowledgements

The researcher would like to thank and express the deepest gratitude to everyone……

Author Contributions: The authors contributed to all parts of the current study.
Funding: This study received no external funding.
Conflicts of Interest: The authors declare no conflict of interest.

References

[1] Lauriat, G., and Ghafir, R., "Forced Convective Heat Transfer in Porous Media," *Handbook of Porous Media, Second Edition*, CRC Press, 2000, pp. 201–267. https://doi.org/10.1201/9780824741501.pt3

[2] Young, T. J., and Vafai, K., "Convective Cooling of a Heated Obstacle in a Channel," *International Journal of Heat and Mass Transfer*, Vol. 41, No. 20, 1998, pp. 3131–3148. https://doi.org/10.1016/S0017-9310(97)00323-2

[3] Kaviany, M., "Laminar Flow through a Porous Channel Bounded by Isothermal Parallel Plates," *International Journal of Heat and Mass Transfer*, Vol. 28, No. 4, 1985, pp. 851–858. https://doi.org/10.1016/0017-9310(85)90234-0

[4] Vafai, K., and Tien, C. L., "Boundary and Inertia Effects on Flow and Heat Transfer in Porous Media," *International Journal of Heat and Mass Transfer*, Vol. 24, No. 2, 1981, pp. 195–203. https://doi.org/10.1016/0017-9310(81)90027-2

[5] Huang, P. C., and Vafai, K., "Analysis of Forced Convection Enhancement in a Channel Using Porous Blocks," *Journal of Thermophysics and Heat Transfer*, Vol. 8, No. 3, 1994, pp. 563–573. https://doi.org/10.2514/3.579

[6] Pavel, B. I., and Mohamad, A. A., "An Experimental and Numerical Study on Heat Transfer Enhancement for Gas Heat Exchangers Fitted with Porous Media," *International Journal of Heat and Mass Transfer*, Vol. 47, No. 23, 2004, pp. 4939–4952. https://doi.org/10.1016/j.ijheatmasstransfer.2004.06.014

[7] Yucel, N., and Guven, R. T., "Forced-Convection Cooling Enhancement of Heated Elements in a Parallel-Plate Channel Using Porous Inserts," *Numerical Heat Transfer, Part A: Applications*, Vol. 51, No. 3, 2007, pp. 293–312. https://doi.org/10.1080/10407780600762533

[8] Itō, H., "Friction Factors for Turbulent Flow in Curved Pipes," *Journal of Basic Engineering*, Vol. 81, No. 2, 1959, pp. 123–132.

[9] Jayakumar, J.S., Mahajani, S.M., Mandal, J. C., Vijayan, P. K., and Bhoi, R., "Experimental and CFD Estimation of Heat Transfer in Helically Coiled Heat Exchangers," *Chemical Engineering Research and Design*, Vol. 86, No. 3, 2008, pp. 221–232. https://doi.org/10.1016/j.cherd.2007.10.021

[10] Jamarani, A., Maerefat, M., and Eshagh Nimvari, M., "Numerical Study of Heat Transfer in Double-Tube Heat Exchanger Filled with Porous Material in a Turbulent Fluid Flow," *mdrsjrns*, Vol. 16, No. 3, 2016, pp. 173–184. http://mme.modares.ac.ir/article-15-2594-fa.html

[11] Rodrigues, M. K., da Silva Brum, R., Vaz, J., Rocha, L. A. O., dos Santos, E. D., and Isoldi, L. A., "Numerical Investigation about the Improvement of the Thermal Potential of an Earth-Air Heat Exchanger (EAHE) Employing the Constructal Design Method," *Renewable Energy*, Vol. 80, 2015, pp. 538–551.

[12] Chen, L., "Progress in Study on Constructal Theory and Its Applications," *Science China Technological Sciences*, Vol. 55, 2012, pp. 802–820.

[13] Babaelahi, M., Sadri, S., and Sayyaadi, H., "Multi-Objective Optimization of a Cross-Flow Plate Heat Exchanger Using Entropy Generation Minimization," *Chemical Engineering & Technology*, Vol. 37, No. 1, 2014, pp. 87–94.

[14] Byrde, O., and Sawley, M. L., "Optimization of a Kenics Static Mixer for Non-Creeping Flow Conditions," *Chemical Engineering Journal*, Vol. 72, No. 2, 1999, pp. 163–169.

[15] Kumar, V., Shirke, V., and Nigam, K. D. P., "Performance of Kenics Static Mixer over a Wide Range of Reynolds Number," *Chemical Engineering Journal*, Vol. 139, No. 2, 2008, pp. 284–295.

[16] Hobbs, D. M., Swanson, P. D., and Muzzio, F. J., "Numerical Characterization of Low Reynolds Number Flow in the Kenics Static Mixer," *Chemical Engineering Science*, Vol. 53, No. 8, 1998, pp. 1565–1584.

[17] Biçer, N., Engin, T., Yaşar, H., Büyükkaya, E., Aydın, A., and Topuz, A., "Design Optimization of a Shell-and-Tube Heat Exchanger with Novel Three-Zonal Baffle by Using CFD and Taguchi Method," *International Journal of Thermal Sciences,* Vol. 155, 2020, p. 106417.
[18] Faridi Khouzestani, R., and Ghafouri, A., "Numerical Study on Heat Transfer and Nanofluid Flow in Pipes Fitted with Different Dimpled Spiral Center Plate," *SN Applied Sciences*, Vol. 2, No. 2, 2020, p. 298.
[19] Li, N., Chen, J., Cheng, T., Klemeš, J. J., Varbanov, P. S., Wang, Q., Yang, W., Liu, X., and Zeng, M., "Analysing Thermal-Hydraulic Performance and Energy Efficiency of Shell-and-Tube Heat Exchangers with Longitudinal Flow Based on Experiment and Numerical Simulation," *Energy*, Vol. 202, 2020, p. 117757.
[20] Zhao, C. Y., Lu, T. J., and Hodson, H. P., "Natural Convection in Metal Foams with Open Cells," *International Journal of Heat and Mass Transfer*, Vol. 48, No. 12, 2005, pp. 2452–2463.
[21] Phanikumar, M. S., and Mahajan, R. L., "Non-Darcy Natural Convection in High Porosity Metal Foams," *International Journal of Heat and Mass Transfer*, Vol. 45, No. 18, 2002, pp. 3781–3793.
[22] Buonomo, B., Diana, A., Manca, O., and Nardini, S., "Local Thermal Non-Equilibrium Investigation on Natural Convection in Horizontal Channel Heated from Above and Partially Filled with Aluminum Foam," *Energy Procedia*, Vol. 126, 2017, pp. 42–49.
[23] Andreozzi, A., Bianco, N., Iasiello, M., and Naso, V., "Numerical Study of Metal Foam Heat Sinks under Uniform Impinging Flow," Vol. 796, 2017, pp. 012002.
[24] Huang, Y., Sun, Q., Yao, F., and Zhang, C., "Experimental Study on the Thermal Performance of a Finned Metal Foam Heat Sink with Phase Change Material," *Heat Transfer Engineering*, Vol. 42, No. 7, 2021, pp. 579–591.
[25] Awais, M., Saad, M., Ayaz, H., Ehsan, M. M., and Bhuiyan, A. A., "Computational Assessment of Nano-Particulate (Al2O3/Water) Utilization for Enhancement of Heat Transfer with Varying Straight Section Lengths in a Serpentine Tube Heat Exchanger," *Thermal Science and Engineering Progress*, Vol. 20, 2020, p. 100521.
[26] Marzouk, S. A., Abou Al-Sood, M. M., El-Said, E. M. S., and El-Fakharany, M. K., "Effect of Wired Nails Circular–Rod Inserts on Tube Side Performance of Shell and Tube Heat Exchanger: Experimental Study," *Applied Thermal Engineering*, Vol. 167, 2020, p. 114696.
[27] Parisher, R. A., "Pipe Drafting and Design," Elsevier, 2001.
[28] Anderson, D., Tannehill, J. C., and Pletcher, R. H., "Computational Fluid Mechanics and Heat Transfer," CRC Press, 2016. https://doi.org/10.1201/b12884
[29] Ehlers, W., and Bluhm, J., Eds., "Porous Media," Springer Berlin Heidelberg, Berlin, Heidelberg, 2002. https://doi.org/10.1007/978-3-662-04999-0
[30] Menter, F. R., Lechner, R., and Matyushenko, A., "Best Practice: Generalized k-ω (GEKO) Two-Equation Turbulence Modeling in Ansys CFD," *ANSYS: Cannon Sburg, PA, USA*, 2021, pp. 1–32.
[31] Menter, F. R., Lechner, R., and Matyushenko, A., "Best Practice: Generalized k-ω Two-Equation Turbulence Model in ANSYS CFD (GEKO)," 2019.
[32] Menter, F. R., Sechner, R., and Matyushenko, A., "Best Practice: RANS Turbulence Modeling in Ansys CFD," *ANSYS Inc.: Canonsburg, PA, USA*, 2021.
[33] ANSYS Inc., "ANSYS Fluent 18.0 Theory Guide."